Synsint Research Group

Available online at www.synsint.com

Synthesis and Sintering

ISSN 2564-0186 (Print), **ISSN** 2564-0194 (Online)

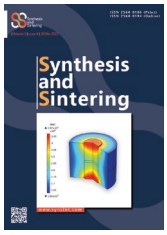

Research article

Is synthesizing a $Cu_{35}Co_{35}Ni_{20}Ti_5Al_5$ high-entropy alloy beyond the rules of solid-solution formation?

Samaneh Mamnooni [a], **Ehsan Borhani** [a,*], **Hassan Heydari** [b]

[a] *Department of New Science and Technology, Nanomaterials Group, Semnan University, Semnan, Iran*
[b] *Department of Materials and Metallurgical Engineering, Semnan University, Semnan, Iran*

A B S T R A C T

In this research, an attempt was made to produce multi-component nanocrystalline $Cu_{35}Co_{35}Ni_{20}Ti_5Al_5$ alloy by mechanical alloying. To produce this high-entropy alloy, the primary powders were milled for 40 h and characterized by XRD, SEM, EDS, and DSC analyses. The milling process has reduced the size of the crystallites to the nanometer scale and a nanostructured multicomponent powder with a crystallite size of 29 nm was obtained. According to the XRD patterns and EDS maps of the milled powder for the longest time, aluminum and copper were homogeneously distributed, cobalt had a less homogeneous distribution than these two elements, but nickel and titanium remained in concentrated spots. Finally, thermodynamic calculations were done to clarify the reason for the impossibility of forming a solid solution for the synthesis of the $Cu_{35}Co_{35}Ni_{20}Ti_5Al_5$ high-entropy alloy.

KEYWORDS

Mechanical alloying
High-entropy alloys
Solid solution
Unsuccessful synthesis
Thermodynamics

OPEN ACCESS

1. Introduction

Alloying is the greatest award of metallurgy to humankind. The invention of new materials has been very important since ancient times because of its impact on human civilization's progress. Since the accidental discovery of alloys in the primeval fires, these materials have been an essential part of materials development [1, 2]. The traditional alloy design scenario is that one or two elements are selected as the basic elements for primary properties and a number of minor elements are added to improve certain properties. Using this traditional path, several alloys like steel and aluminum alloys have been advanced [3–5].

High-entropy alloys (HEAs) were introduced almost simultaneously by Cantor et al. [3] and Yeh et al. [5], which led to a significant growth in the development of alloys. They introduced HEAs as alloys consisting of at least 5 principal elements with contents between 5% and 35%. The high entropy of the components in these alloys results in the synthesis of a simple solid solution instead of complex phases because of the high mixing entropy effect [6].

To produce a high-entropy alloy, several key factors and elemental properties play crucial roles in the characteristics of the alloy. HEAs are characterized by their unique composition, typically comprising multiple principal elements in approximately equiatomic or near-equiatomic ratios. The size mismatch and electronegativity of the constituent elements play significant impacts [7–9]. The combination of elements with varying atomic sizes and electronegativities contributes to the high configurational entropy of HEAs, which boosts their solid solution behavior [10, 11]. Additionally, the mixing enthalpy is another crucial parameter that influences the phase formation and thermodynamic stability of HEAs. Elements with different crystal structures and electronic configurations can lead to the formation of solid solution phases, thereby contributing to the high entropy effect [12–14].

Yeh [15] introduced four core effects as characteristics of properties and microstructure of high-entropy alloys including high configurational entropy, sluggish diffusion, lattice distortion, and the cocktail effect [15–17]. The appealing properties of high-entropy alloys such as great strength [18], high fracture toughness at low temperatures

* Corresponding author. *E-mail address:* e.borhani@semnan.ac.ir (E. Borhani)
Received 9 September 2023; Received in revised form 9 November 2023; Accepted 15 November 2023.

https://doi.org/10.53063/synsint.2023.34177

[19], and admirable oxidation and corrosion resistance [20–22] have made these materials a popular choice for most engineering applications [23–27]. It should be noted that the crystallographic lattice of a HEA determines its mechanical properties [28].

Several methods can be used to synthesize HEAs such as vacuum arc melting, rapid solidification, and mechanical alloying (MA) [29]. In addition to bulk HEAs, which have been widely produced, nanocrystalline HEAs have also been expanding recently. Being nanocrystalline increases the excitement of the vast composition area and elaborate applicability of the HEAs. Good magnetic behavior, enhanced mechanical properties, and great thermal stability are characteristic of nanocrystalline HEAs [30–32].

High-energy ball milling or mechanical alloying is a solid-state and non-equilibrium technique, which can be applied to achieve a stable microstructure with better homogeneity and nanocrystalline structure. The basis of this process is the milling of elemental powder particles to obtain alloying at atomic scale. The procedure of manufacturing different materials by the MA method includes repeated fracturing and cold welding of powders entrapped between the milling media and the balls, the expansion of which is related to the mechanical properties of powder components [33].

Although the MA route was originally developed for oxide dispersion strengthened (ODS) alloys [34], it was successfully used to fabricate a wide range of materials such as solid solution alloys, ordered compounds, intermetallics, and nanocomposites [35]. Mechanical alloying can also increase solid solubility even in immiscible systems. Dissimilar to chemical techniques and decomposition routes for manufacturing nanomaterials, extensive synthesis of powder is appropriate over the MA employing machines like planetary ball mill [33].

The present study focuses on the possible synthesis of $Cu_{35}Co_{35}Ni_{20}Ti_5Al_5$ high-entropy alloy through mechanical alloying. The formation of structures, phase evaluation during mechanical alloying, and thermal stability are also studied. The feasibility of producing this HEA is also evaluated by thermodynamic calculations considering the principles of solid solution formation.

2. Experimental procedure

Nanocrystalline $Cu_{35}Co_{35}Ni_{20}Ti_5Al_5$ high-entropy alloy was tried to be prepared through mechanical alloying of certain values of elemental powders of Cu, Co, Ni, Ti, and Al. The purity of all metal raw materials was above 99%. Figs. 1 and 2 show the SEM micrographs and XRD patterns of the mentioned elemental powders, respectively. Mechanical alloying was conducted with a high-energy planetary ball mill (Retsch PM 100) with tungsten carbide balls and toluene as a process control agent. Ball to powder weight ratio (BPR) was equal to 10:1. This work was performed under an argon atmosphere at a speed of 200 rpm for 10, 20, 30, and 40 h.

The phase analysis was done by XRD on the milled powders using a Philips PW3710 diffractometer with Co K_α radiation (1.78 Å) at a scan step of 0.02 °. Crystallite size calculations were performed by X'Pert HighScore Plus software. An FEI ESEM Quanta 200 scanning electron microscope (SEM) equipped with an energy-dispersive spectroscope (EDS) was used to investigate the effect of milling on the microstructure and chemical composition of the 40-h milled powder sample, respectively. Differential scanning calorimetry (DSC) was carried out using TA-1A Pishtaz Engineering Co. apparatus with a heating rate of 10 °C/min up to 1300 °C in an argon atmosphere to analyze the thermal behavior of the 40-h milled specimen.

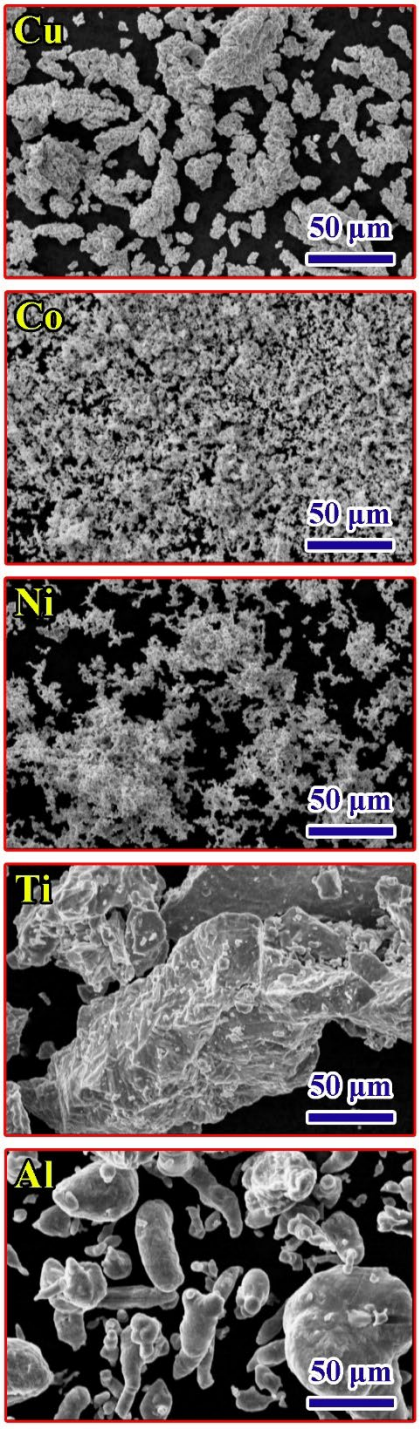

Fig. 1. SEM images of the used elemental powders.

3. Results and discussion

The XRD patterns of the $Cu_{35}Co_{35}Ni_{20}Ti_5Al_5$ powders for various milling times are shown in Fig. 3. It can be observed that with the

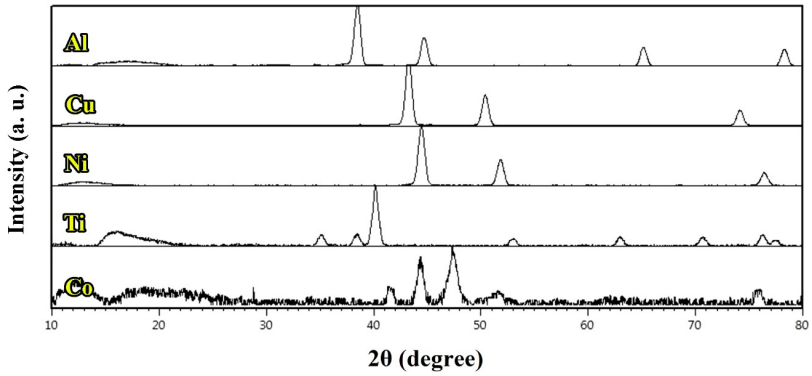

Fig. 2. XRD patterns of the used elemental powders.

increase of the milling time, the intensity of the peaks related to each element is significantly reduced and some broadening of the peak is observed. However, increasing the milling time has not been able to remove the peaks related to the elements. The drop in the intensity of the peaks and their broadening is attributed to the decrease in crystallite size and formation of nanocrystalline structure, high lattice strain, and refined crystal structure due to milling [29, 36, 37].

The alloying process during mechanical alloying can be considered similar to that in traditional diffusion coupling, while unlike traditional diffusion coupling, the scale is micrometer in mechanical alloying and the diffusion is carried out through strain in the milled powder [38]. Also, most of the milling time was not effective in approaching the peaks and merging them with each other or in the disappearance of the diffraction peaks, which is a sign of no solid solution formation [16, 36, 39]. By comparing the peaks in the XRD patterns for different milling times, it can be pointed out that the intensity of the Al peaks decreases sharply than the peaks of the other four elements. In addition, the intensity of the peaks related to Cu lessens more than the other three elements of Ti, Ni, and Co. The next rank in the reduction of peak intensity is attributed to the Co. The findings of XRD patterns are confirmed by EDS elemental mapping in the following sections. However, the trends seen in diminishing peaks of Al and Cu may be associated with the softer structure of these metals. The Ti is several times harder and has a higher melting temperature, so it may not be dispersed and cold-welded, due to insufficient milling energy.

The size of crystallites was measured at different times of milling using XRD patterns and X'Pert HighScore Plus software, which uses Scherer's formula (Eq. 1) to calculate crystallite sizes. Scherer's formula expresses the relationship between crystallite size (D) and the wavelength of incident rays (λ), the diffraction angle (θ), and the full

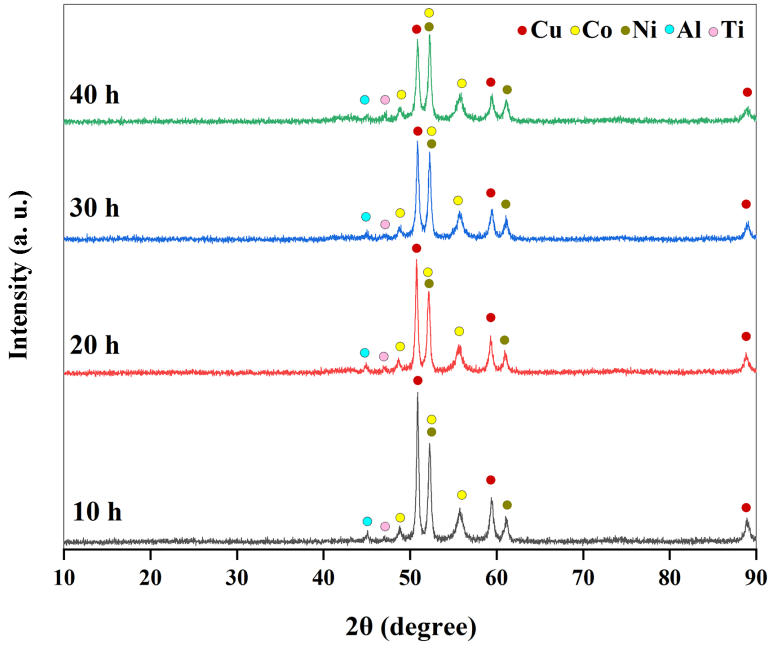

Fig. 3. XRD patterns of $Cu_{35}Co_{35}Ni_{20}Ti_5Al_5$ milled powders based on various milling times.

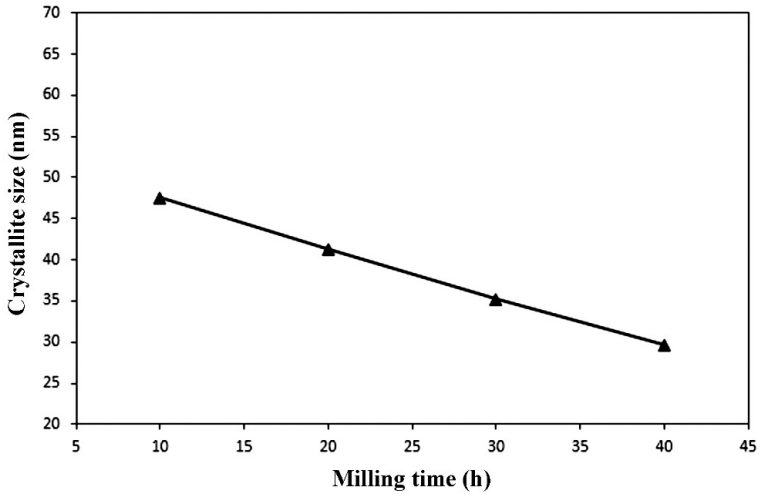

Fig. 4. Variation of crystallite size of $Cu_{35}Co_{35}Ni_{20}Ti_5Al_5$ powders by milling time.

width at half maximum intensity (β). According to Fig. 4, which shows the variations in the crystallite size versus the milling time, it is obvious that with enhancing milling time, this parameter decreases. Such a trend can be predictable due to the repeated recrystallization during the MA process [40].

$$D = \frac{0.9\lambda}{\beta \mathrm{Cos}\,\theta} \quad (1)$$

In addition to the XRD test, SEM/EDS analyses were employed to study the local microstructure and dispersion of the five elements in the target HEA. The SEM image and the results of EDS map analysis of the desired $Cu_{35}Co_{35}Ni_{20}Ti_5Al_5$ sample after milling for 40 h are shown in Figs. 5 and 6, respectively. According to the EDS elemental mapping, it is clear that aluminum and copper were homogeneously distributed, and cobalt had a less homogeneous distribution than these two elements. However, nickel and titanium remained in relatively segregated spots. Among nickel and titanium, nickel showed a more homogeneous dispersion than titanium.

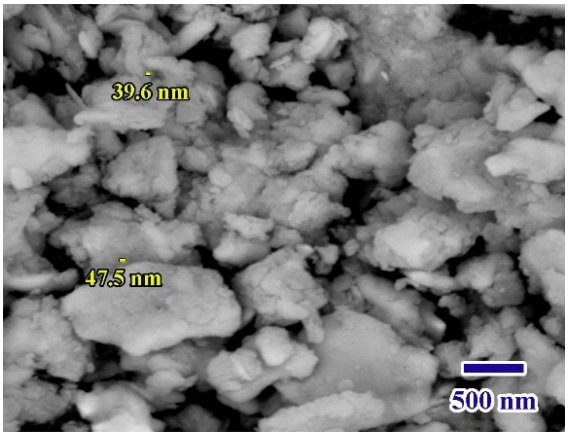

Fig. 5. SEM image of $Cu_{35}Co_{35}Ni_{20}Ti_5Al_5$ powder mixture after milling for 40 h.

It seems that cobalt, nickel, and titanium need more time to disperse and become uniform, and the milling duration may not be long enough to create such a uniform microstructure. The findings of this study are consistent with the results reported in Ref. [38], which investigated the alloying of different elements in a composition similar to the present work, but with an order of Al→Cu→Co→Ni→Ti. In the mentioned research, it was shown that the order of the alloying progress of the basic elements of an alloy over milling is predictable with the alloying stages. Among the important influential metallurgical factors such as crystal structure, melting point, atomic size, and self-diffusion coefficient, the melting point was introduced as the most important factor in the alloy sequence in that system of elements [38].

In another study on the production of AlMgNiCrTi high-entropy alloy, the effect of melting points on the alloy sequence of different elements was confirmed [41]. Similar to the diffusion theory of conventional alloy systems, which states a close relationship between the coefficient of diffusion and the melting point, this relevance can be extended to the element's intrinsic diffusion in a material with polybasic elements [38, 42].

In addition to the role of diffusion, the effect of mechanical fragmentation and structural deformation of the basic elements should be considered because it is also affected by the melting point. In fact, a metal with a lower melting temperature will have better malleability and lower hardness, so it will have better distribution. This means that metals with higher malleability like aluminum and copper, are dispersed faster in the early stages of milling, and are diffused rapidly into other elements and phases in later stages [38].

Although the melting point of cobalt is higher than that of nickel, the tendency of this element to form an alloy is higher than that of nickel. Considering the similar diffusion coefficient of these two elements, a mechanical factor can be used to explain this reverse trend. Additionally, the fewer slip systems in the HCP structure of the cobalt, make this element more brittle than nickel, so cobalt breaks and disperses faster than nickel during milling. Thus, the melting temperature is considered the main factor in determining the dispersion rate of a metal, but for elements with relatively similar melting points, other factors such as crystalline structure will be important [38].

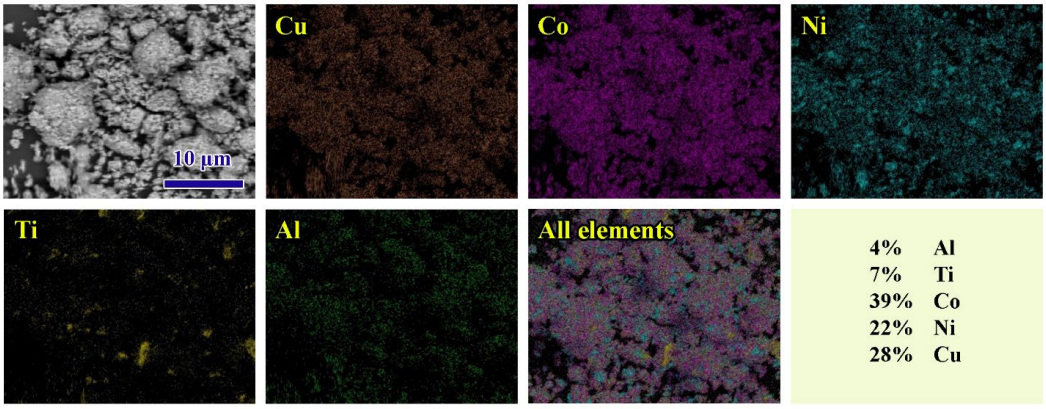

Fig. 6. EDS map analysis of $Cu_{35}Co_{35}Ni_{20}Ti_5Al_5$ powder mixture after milling for 40 h.

Fig. 7 shows the DSC curve of the $Cu_{35}Co_{35}Ni_{20}Ti_5Al_5$ HEA target, milled for 40 h, with a heating rate of 10 °C/min up to 1300 °C. In this analysis, which is a thermal analytical technique, the amount of heat needed to intensify the temperature of the original sample and the reference sample is measured as a function of temperature, and thermal stability is determined based on exothermic and endothermic reactions [41]. According to the DSC results, it is clear that the sample had a slight endothermic trend close to zero in the entire range of analysis. The absence of a specific endothermic peak indicates that the melting point of the synthesized powder is higher than 1300 °C, even though the melting points of Al and Cu are 660 °C and 1083 °C, respectively. Therefore, the milled powder is thermally stable up to at least 1300 °C. It should be reminded that the melting temperature of nickel, cobalt, and titanium are 1453 °C, 1495 °C, and 1660 °C, respectively.

According to the results of the above-mentioned experimental observations and scientific discussions, it can be stated that the synthesis of $Cu_{35}Co_{35}Ni_{20}Ti_5Al_5$ high-entropy alloy and the formation of a solid solution is not possible. In the following, the thermodynamic principles and the rules governing the formation of solid solutions will be discussed to clarify the reasons for the failure in the HEA synthesis. Yeh et al. [5] explained formation of HEAs through the ΔS_{mix} parameter, which can be calculated from Eq. 2 [5, 43]:

$$\Delta S_{mix} = -R\sum_{i=1}^{n}(c_i \ln c_i) \quad (2)$$

where R is the universal gas constant (8.314 $J.k^{-1}.mol^{-1}$), n shows the number of components, and c_i is the atomic percentage related to the i^{th} component. At the beginning of the invention of HEAs, the condition of $\Delta S_{mix} \geq 13.38$ $J.k^{-1}.mol^{-1}$ seemed to be sufficient to obtain a high-entropy alloy without the synthesis of any intermetallic or other complex phases [5, 43, 44]. Higher ΔS_{mix} would reduce ΔG_{mix} parameter based on $\Delta G_{mix} = \Delta H_{mix} - T\Delta S_{mix}$ relationship, where ΔG_{mix} represents the Gibbs free energy of mixing and ΔH_{mix} is the enthalpy of

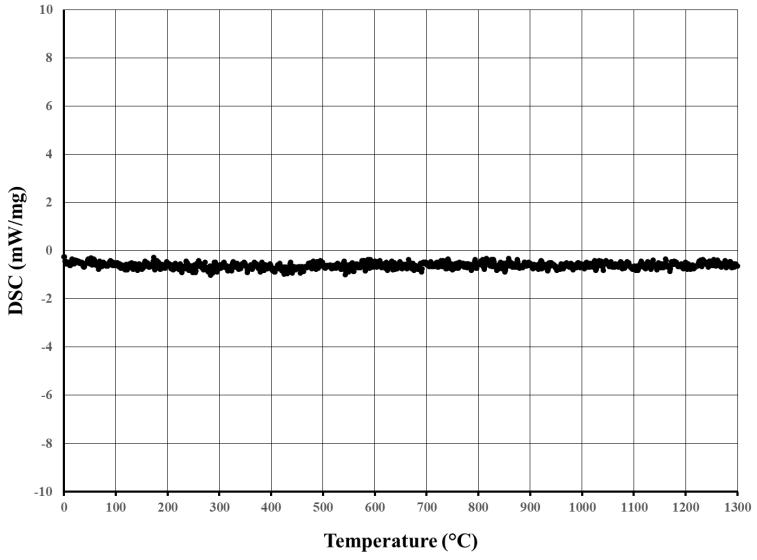

Fig. 7. DSC analysis of the 40-h milled $Cu_{35}Co_{35}Ni_{20}Ti_5Al_5$ sample heated up to 1300 °C.

mixing. Later it was proved that the higher amount of ΔS_{mix} parameter does not necessarily reduce ΔG_{mix} value and the $\Delta S_{mix} \geq 13.38$ J.k^{-1}.mol^{-1} condition is not enough to achieve a HEA solid solution [43, 45, 46].

To predict the certainty of the formation of a HEA solid solution, the conditions of $\delta r \leq 6.6\%$ (atomic size difference) and $\Omega \geq 1.1$ (scaled ratio of ΔS_{mix} to ΔH_{mix}) should be examined [47]:

$$\delta r = \sqrt{\sum_{i=1}^{n} c_i (1 - r_i / \sum_{i=1}^{n} c_i r_i)^2} \quad (3)$$

$$\Omega = \frac{T_m \Delta S_{mix}}{|\Delta H_{mix}|} \quad (4)$$

where r_i represents the atomic radius of the ith component and $T_m = \sum_{i=1}^{n} c_i (T_m)_i$, $(T_m)_i$ is the melting point of ith constituent element [47]. Pauling electronegativity difference ($\delta\chi$) and ΔH_{mix} parameters can be calculated using Eqs. 5 and 6, respectively [47,48]:

$$\delta\chi = \sqrt{\sum_{i=1}^{n} c_i (\chi_i - \sum_{i=1}^{n} c_i \chi_i)^2} \quad (5)$$

$$\Delta H_{mix} = \sum_{i=1, i \neq j}^{n} 4 \Delta H_{ij}^{mix} c_i c_j \quad (6)$$

where χ_i is the electronegativity of the ith constituent, c_j is the atomic percentage related to the jth component, and ΔH_{ij}^{mix} represents the enthalpy of mixing related to the ith and jth components [47, 48].

The simulation results for the $Cu_{35}Co_{35}Ni_{20}Ti_5Al_5$ high-entropy alloy are summarized in Table 1. According to these calculations, the values of ΔS_{mix}, ΔH_{mix}, δr, $\delta\chi$, Ω and T_m parameters for the $Cu_{35}Co_{35}Ni_{20}Ti_5Al_5$ sample are 11.28 J.k^{-1}.mol^{-1}, -2.51 kJ.mol^{-1}, 4.49%, 0.097%, 7.11 and 1583 K (1310 °C), respectively. Based on the calculated value for the ΔS_{mix} parameter (11.28 J.k^{-1}.mol^{-1}), the initial condition for the synthesis of the $Cu_{35}Co_{35}Ni_{20}Ti_5Al_5$ solid solution ($\Delta S_{mix} \geq 13.38$ J.k^{-1}.mol^{-1}) was not satisfied. Hence, obtaining the target high-entropy alloy is not possible thermodynamically.

Table 1. Simulation results of alloy composition.

		Element 1	Element 2	Element 3	Element 4	Element 5	
Elements		Ni	Co	Cu	Al	Ti	
Element 1	Ni	Ni	0	4	-22	-35	
Element 2	Co		Co	6	-19	-28	
Element 3	Cu			Cu	-1	-9	
Element 4	Al				Al	-30	
Element 5	Ti					Ti	
		Element 1	**Element 2**	**Element 3**	**Element 4**	**Element 5**	
		Ni	Co	Cu	Al	Ti	
Atomic size (Å)		1.246	1.251	1.278	1.431	1.461	
Composition fraction		0.2	0.35	0.35	0.05	0.05	1
		0.2492	0.43785	0.4473	0.07155	0.07305	1.27895
		1.33E-04	1.67E-04	1.93E-07	7.07E-04	1.01E-03	2.02E-03
Atomic size difference (%)							4.4943098
Melting point (K)		1728	1768	1358	933	1941	
		345.6	618.8	475.3	46.65	97.05	1583.4
Melting point (K)							1583.4
Electronegativity		1.91	1.88	1.9	1.61	1.54	
		0.382	0.658	0.665	0.0805	0.077	1.8625
		0.000451	0.000107	0.000492	3.19E-03	0.0052	0.00943875
Pauling electronegativity difference							0.09715349
VEC		10	9	11	3	4	
		2	3.15	3.85	0.15	0.2	9.35
VEC							9.35
Enthalpy of mixing (kJ/mol)							-2.51
Entropy of mixing (J/mol.K)							11.27658
Omega							7.11368

Changes in the value of the ΔH_{mix} parameter from zero to negative increase the probability of intermetallic phase formation [49]. Therefore, according to the value of the ΔH_{mix} parameter (-2.51 kJ.mol^{-1}), the formation of small amounts of intermetallic phases can be predicted for the $Cu_{35}Co_{35}Ni_{20}Ti_5Al_5$ composition.

Finally, for the prediction of the solid solution crystalline structure, the valence electron concentration (VEC) parameter is computed according to Eq. 7:

$$VEC = \sum_{i=1}^{n} c_i (VEC)_i \quad (7)$$

where VEC_i is the VEC of the i^{th} component. If VEC ≥ 8, the final structure will have an FCC lattice [50, 51]. According to Table 1, a value of 9.35 is calculated for the VEC parameter of the $Cu_{35}Co_{35}Ni_{20}Ti_5Al_5$ composition.

4. Conclusions

A study was done to synthesize multi-component $Cu_{35}Co_{35}Ni_{20}Ti_5Al_5$ high-entropy alloy by mechanical alloying. The application of the milling process reduced the size of the crystallites to the nanoscale. On the basis of the results of the XRD test, the elimination of elemental peaks and complete diffusion of elements into each other were not successful. The results of the EDS analysis showed a homogeneous distribution of Al and Cu, a relatively homogeneous distribution of Co, and a heterogeneous distribution of Ni and Ti. The DSC analysis on the 40-h milled powder showed that the melting point of the prepared sample was higher than 1300 °C. A thermodynamic approach was employed to disclose the reason for the impossibility of the synthesis of the $Cu_{35}Co_{35}Ni_{20}Ti_5Al_5$ high-entropy alloy and the formation of a solid solution.

CRediT authorship contribution statement

Samaneh Mamnooni: Writing – original draft, Investigation, Formal Analysis, Data curation, Methodology.
Ehsan Borhani: Writing – review & editing, Supervision.
Hassan Heydari: Writing – review & editing.

Data availability

The data underlying this article will be shared on reasonable request to the corresponding author.

Declaration of competing interest

The authors declare no competing interests.

Funding and acknowledgment

The content of this article is drawn from the doctoral dissertation of the first author, supported by grant number 13792. The authors express their gratitude to Semnan University.

References

[1] B.S. Murty, J.-W. Yeh, S. Ranganathan, P.P. Bhattacharjee, High-entropy alloys, 2nd ed., Elsevier. (2019).
[2] M. Murali, S.P.K. Babu, B.J. Krishna, A. Vallimanalan, Synthesis and characterization of AlCoCrCuFeZnx high-entropy alloy by mechanical alloying, Prog. Nat. Sci. Mater. Int. 26 (2016) 380–384. https://doi.org/10.1016/j.pnsc.2016.06.008.
[3] B. Cantor, I.T.H. Chang, P. Knight, A.J.B. Vincent, Microstructural development in equiatomic multicomponent alloys, Mater. Sci. Eng. A. 375–377 (2004) 213–218. https://doi.org/10.1016/j.msea.2003.10.257.
[4] C.-Y. Hsu, J.-W. Yeh, S.-K. Chen, T.-T. Shun, Wear resistance and high-temperature compression strength of Fcc CuCoNiCrAl0.5Fe alloy with boron addition, Metall. Mater. Trans. A. 35 (2004) 1465–1469. https://doi.org/10.1007/s11661-004-0254-x.
[5] J.-W. Yeh, S.-K. Chen, S.-J. Lin, J.-Y. Gan, T.-S. Chin, et al., Nanostructured high-entropy alloys with multiple principal elements: novel alloy design concepts and outcomes, Adv. Eng. Mater. 6 (2004) 299–303. https://doi.org/10.1002/adem.200300567.
[6] K.-Y. Tsai, M.-H. Tsai, J.-W. Yeh, Sluggish diffusion in Co–Cr–Fe–Mn–Ni high-entropy alloys, Acta Mater. 61 (2013) 4887–4897. https://doi.org/10.1016/j.actamat.2013.04.058.
[7] E.J. Pickering, N.G. Jones, High-entropy alloys: a critical assessment of their founding principles and future prospects, Int. Mater. Rev. 61 (2016) 183–202. https://doi.org/10.1080/09506608.2016.1180020.
[8] H.J. Jiang, C.Y. Liu, B. Zhang, P. Xue, Z.Y. Ma, et al., Simultaneously improving mechanical properties and damping capacity of Al-Mg-Si alloy through friction stir processing, Mater. Charact. 131 (2017) 425–430. https://doi.org/10.1016/j.matchar.2017.07.037.
[9] M. Li, H. Gao, J. Liang, S. Gu, W. You, et al., Microstructure evolution and properties of graphene nanoplatelets reinforced aluminum matrix composites, Mater. Charact. 140 (2018) 172–178. https://doi.org/10.1016/j.matchar.2018.04.007.
[10] R. Feng, P.K. Liaw, M.C. Gao, M. Widom, First-principles prediction of high-entropy-alloy stability, npj Comput. Mater. 3 (2017) 50. https://doi.org/10.1038/s41524-017-0049-4.
[11] J.-W. Yeh, Alloy design strategies and future trends in high-entropy alloys, JOM. 65 (2013) 1759–1771. https://doi.org/10.1007/s11837-013-0761-6.
[12] R. Li, L. Xie, W.Y. Wang, P.K. Liaw, Y. Zhang, High-throughput calculations for high-entropy alloys: A brief review, Front. Mater. 7 (2020) 290. https://doi.org/10.3389/fmats.2020.00290.
[13] S.B. Li, C.B. Wang, L. Li, Q. Shen, L.M. Zhang, Effect of annealing temperature on structural and electrical properties of BCZT ceramics prepared by Plasma Activated Sintering, J. Alloys Compd. 730 (2018) 182–190. https://doi.org/10.1016/j.jallcom.2017.09.310.
[14] C. Niu, A.J. Zaddach, C.C. Koch, D.L. Irving, First principles exploration of near-equiatomic NiFeCrCo high entropy alloys, J. Alloys Compd. 672 (2016) 510–520. https://doi.org/10.1016/j.jallcom.2016.02.108.
[15] J.-W. Yeh, Recent progress in high-entropy alloys, Ann. Chim. Sci. Des. Mater. 31 (2006) 633–648.
[16] J.-W. Yeh, S.-Y. Chang, Y.-D. Hong, S.-K. Chen, S.-J. Lin, Anomalous decrease in X-ray diffraction intensities of Cu–Ni–Al–Co–Cr–Fe–Si alloy systems with multi-principal elements, Mater. Chem. Phys. 103 (2007) 41–46. https://doi.org/10.1016/j.matchemphys.2007.01.003.
[17] M. Vaidya, S. Trubel, B.S. Murty, G. Wilde, S.V. Divinski, Ni tracer diffusion in CoCrFeNi and CoCrFeMnNi high entropy alloys, J. Alloys Compd. 688 (2016) 994–1001. https://doi.org/10.1016/j.jallcom.2016.07.239.
[18] Z. Li, K.G. Pradeep, Y. Deng, D. Raabe, C.C. Tasan, Metastable high-entropy dual-phase alloys overcome the strength–ductility trade-off, Nature. 534 (2016) 227–230. https://doi.org/10.1038/nature17981.
[19] B. Gludovatz, A. Hohenwarter, D. Catoor, E.H. Chang, E.P. George, R.O. Ritchie, A fracture-resistant high-entropy alloy for cryogenic applications, Science. 345 (2014) 1153–1158. https://doi.org/10.1126/science.1254581.

[20] T.M. Butler, J.P. Alfano, R.L. Martens, M.L. Weaver, High-temperature oxidation behavior of Al-Co-Cr-Ni-(Fe or Si) multicomponent high-entropy alloys, JOM. 67 (2015) 246–259. https://doi.org/10.1007/s11837-014-1185-7.
[21] G. Laplanche, U.F. Volkert, G. Eggeler, E.P. George, Oxidation behavior of the CrMnFeCoNi high-entropy alloy, Oxid. Met. 85 (2016) 629–645. https://doi.org/10.1007/s11085-016-9616-1.
[22] J.H. Zhao, X.L. Ji, Y.P. Shan, Y. Fu, Z. Yao, On the microstructure and erosion–corrosion resistance of AlCrFeCoNiCu high-entropy alloy via annealing treatment, Mater. Sci. Technol. 32 (2016) 1271–1275. https://doi.org/10.1080/02670836.2015.1116494.
[23] R. Sriharitha, B.S. Murty, R.S. Kottada, Phase formation in mechanically alloyed AlxCoCrCuFeNi (x = 0.45, 1, 2.5, 5 mol) high entropy alloys, Intermetallics. 32 (2013) 119–126. https://doi.org/10.1016/j.intermet.2012.08.015.
[24] W. Zhang, P.K. Liaw, Y. Zhang, Science and technology in high-entropy alloys, Sci. China Mater. 61 (2018) 2–22. https://doi.org/10.1007/s40843-017-9195-8.
[25] X.F. Wang, Y. Zhang, Y. Qiao, G.L. Chen, Novel microstructure and properties of multicomponent CoCrCuFeNiTix alloys, Intermetallics. 15 (2007) 357–362. https://doi.org/10.1016/j.intermet.2006.08.005.
[26] Y.J. Zhou, Y. Zhang, Y.L. Wang, G.L. Chen, Solid solution alloys of AlCoCrFeNiTix with excellent room-temperature mechanical properties, Appl. Phys. Lett. 90 (2007). https://doi.org/10.1063/1.2734517.
[27] Y. Zhang, Y.J. Zhou, J.P. Lin, G.L. Chen, P.K. Liaw, Solid-solution phase formation rules for multi-component alloys, Adv. Eng. Mater. 10 (2008) 534–538. https://doi.org/10.1002/adem.200700240.
[28] Ł. Rogal, J. Morgiel, Z. Świątek, F. Czerwiński, Microstructure and mechanical properties of the new Nb25Sc25Ti25Zr25 eutectic high entropy alloy, Mater. Sci. Eng. A. 651 (2016) 590–597. https://doi.org/10.1016/j.msea.2015.10.071.
[29] C.S. babu, K. Sivaprasad, V. Muthupandi, J.A. Szpunar, Characterization of nanocrystalline AlCoCrCuNiFeZn high entropy alloy produced by mechanical alloying, Procedi Mater. Sci. 5 (2014) 1020–1026. https://doi.org/10.1016/j.mspro.2014.07.392.
[30] Y. Zhang, T. Zuo, Y. Cheng, P.K. Liaw, High-entropy alloys with high saturation magnetization, electrical resistivity and malleability, Sci. Rep. 3 (2013) 1455. https://doi.org/10.1038/srep01455.
[31] B. Schuh, F. Mendez-Martin, B. Völker, E.P. George, H. Clemens, et al., Mechanical properties, microstructure and thermal stability of a nanocrystalline CoCrFeMnNi high-entropy alloy after severe plastic deformation, Acta Mater. 96 (2015) 258–268. https://doi.org/10.1016/j.actamat.2015.06.025.
[32] S. Praveen, J. Basu, S. Kashyap, R.S. Kottada, Exceptional resistance to grain growth in nanocrystalline CoCrFeNi high entropy alloy at high homologous temperatures, J. Alloys Compd. 662 (2016) 361–367. https://doi.org/10.1016/j.jallcom.2015.12.020.
[33] B.S. Murty, S. Ranganathan, Novel materials synthesis by mechanical alloying/milling, Int. Mater. Rev. 43 (1998) 101–141. https://doi.org/10.1179/imr.1998.43.3.101.
[34] J.S. Benjamin, T.E. Volin, The mechanism of mechanical alloying, Metall. Trans. 5 (1974) 1929–1934. https://doi.org/10.1007/BF02644161.
[35] C. Suryanarayana, Mechanical alloying and milling, Prog. Mater. Sci. 46 (2001) 1–184. https://doi.org/10.1016/S0079-6425(99)00010-9.
[36] C. Wang, W. Ji, Z. Fu, Mechanical alloying and spark plasma sintering of CoCrFeNiMnAl high-entropy alloy, Adv. Powder Technol. 25 (2014) 1334–1338. https://doi.org/10.1016/j.apt.2014.03.014.
[37] K.B. Zhang, Z.Y. Fu, J.Y. Zhang, W.M. Wang, S.W. Lee, K. Niihara, Characterization of nanocrystalline CoCrFeNiTiAl high-entropy solid solution processed by mechanical alloying, J. Alloys Compd. 495 (2010) 33–38. https://doi.org/10.1016/j.jallcom.2009.12.010.
[38] Y.-L. Chen, Y.-H. Hu, C.-A. Hsieh, J.-W. Yeh, S.-K. Chen, Competition between elements during mechanical alloying in an octonary multi-principal-element alloy system, J. Alloys Compd. 481 (2009) 768–775. https://doi.org/10.1016/j.jallcom.2009.03.087.
[39] K.B. Zhang, Z.Y. Fu, J.Y. Zhang, W.M. Wang, H. Wang, et al., Microstructure and mechanical properties of CoCrFeNiTiAl high-entropy alloys, Mater. Sci. Eng. A. 508 (2009) 214–219. https://doi.org/10.1016/j.msea.2008.12.053.
[40] Y.-L. Chen, Y.-H. Hu, C.-W. Tsai, C.-A. Hsieh, S.-W. Kao, et al., Alloying behavior of binary to octonary alloys based on Cu–Ni–Al–Co–Cr–Fe–Ti–Mo during mechanical alloying, J. Alloys Compd. 477 (2009) 696–705. https://doi.org/10.1016/j.jallcom.2008.10.111.
[41] A.M. Rameshbabu, P. Parameswaran, V. Vijayan, R. Panneer, Diffraction, microstructure and thermal stability analysis in a double phase nanocrystalline Al20Mg20Ni20Cr20Ti20 high entropy alloy, J. Mech. Behav. Mater. 26 (2017) 127–132. https://doi.org/10.1515/jmbm-2017-0021.
[42] J.-W. Yeh, S.-J. Lin, T.-S. Chin, J.-Y. Gan, S.-K. Chen, et al., Formation of simple crystal structures in Cu-Co-Ni-Cr-Al-Fe-Ti-V alloys with multiprincipal metallic elements, Metall. Mater. Trans. A. 35 (2004) 2533–2536. https://doi.org/10.1007/s11661-006-0234-4.
[43] Y. Zhang, T.T. Zuo, Z. Tang, M.C. Gao, K.A. Dahmen, et al., Microstructures and properties of high-entropy alloys, Prog. Mater. Sci. 61 (2014) 1–93. https://doi.org/10.1016/j.pmatsci.2013.10.001.
[44] M.-H. Tsai, J.-W. Yeh, High-entropy alloys: A critical review, Mater. Res. Lett. 2 (2014) 107–123. https://doi.org/10.1080/21663831.2014.912690.
[45] T.-T. Shun, L.-Y. Chang, M.-H. Shiu, Microstructure and mechanical properties of multiprincipal component CoCrFeNiMox alloys, Mater. Charact. 70 (2012) 63–67. https://doi.org/10.1016/j.matchar.2012.05.005.
[46] T.-T. Shun, L.-Y. Chang, M.-H. Shiu, Microstructures and mechanical properties of multiprincipal component CoCrFeNiTix alloys, Mater. Sci. Eng. A. 556 (2012) 170–174. https://doi.org/10.1016/j.msea.2012.06.075.
[47] D.B. Miracle, O.N. Senkov, A critical review of high entropy alloys and related concepts, Acta Mater. 122 (2017) 448–511. https://doi.org/10.1016/j.actamat.2016.08.081.
[48] H. Heydari, M. Tajally, A. Habibolahzadeh, Computational analysis of novel AlLiMgTiX light high entropy alloys, Mater. Chem. Phys. 280 (2022) 125834. https://doi.org/10.1016/j.matchemphys.2022.125834.
[49] V. Shivam, J. Basu, Y. Shadangi, M.K. Singh, N.K. Mukhopadhyay, Mechano-chemical synthesis, thermal stability and phase evolution in AlCoCrFeNiMn high entropy alloy, J. Alloys Compd. 757 (2018) 87–97. https://doi.org/10.1016/j.jallcom.2018.05.057.
[50] S. Guo, C. Ng, J. Lu, C.T. Liu, Effect of valence electron concentration on stability of fcc or bcc phase in high entropy alloys, J. Appl. Phys. 109 (2011). https://doi.org/10.1063/1.3587228.
[51] S. Guo, C.T. Liu, Phase stability in high entropy alloys: Formation of solid-solution phase or amorphous phase, Prog. Nat. Sci. Mater. Int. 21 (2011) 433–446. https://doi.org/10.1016/S1002-0071(12)60080-X.